On Analytical Study of the Self-Affine Mapping System in the Image Processing Domain

M. Saadatmand-Tarzjan*, H. Ghassemian**

*Department of Electrical Engineering, Tarbiat Modares University, *saadatmand@kiaeee.org*
**Department of Electrical Engineering, Tarbiat Modares University, *ghassemi@modares.ac.ir*

Abstract: *All image processing applications of the self-affine mapping system (SAMS) were developed based on the attraction and repellence behaviours. In this paper, we provide some analytical justifications for these properties. Besides, it is shown that the cost function of SAMS sometimes have multiple equivalent solutions which may produce ambiguity. We improve the cost function of self-affine snake as an application of SAMS in the image processing domain. Experimental results demonstrate its results for a number of medical images.*

Keywords: Self-Affine Mapping System, Analytical Study, Self-Affine Snake, Medical Image Segmentation.

1. Introduction

The self-affine mapping system (SAMS) was typically used for producing fractal figures [1-2] and fractal image coding [3]. Ida and Sambonsugi [4] investigated attraction and repellence behaviors of self-affine maps. In more details, they showed that the points mapped by a contractive (expanding) self-affine map are attracted (repelled) by the edges images. The above findings were employed to provide a number of image processing algorithms such as image segmentation and edge detection [4]. Then, they used contractive self-affine maps for contour extraction in order to closely fit a self-affine curve to the desired boundaries with concavities and sharp corners [5]. However, the curve sometimes abnormally deformed due to fractal behavior. In another work, the authors tackled this problem by defining the contour as a primary parametric curve [7]. Recently, they proposed self-affine snake (SAS) which integrates SAMS, wavelet transform, and parametric active contours to keep strengths and avoid weak points [6].

However, all the above promising applications of SAMS in the image processing domain were based on Ida's experimental findings about the attraction and repellence behaviors. Though, the lake of an analytical justification is actually felt.

In this paper, we analytically study the properties of self-affine maps and provide three lemmas to describe their behaviors. Furthermore, the cost function of SAS is improved and then, its results for a number of medical images are illustrated in the experimental results.

The paper is organized as follows. In Section 2, self-affine mapping system is briefly introduced. Section 3 is devoted to analytical justifications. In Section 4, we introduce self-affine snake and improve its cost function. Section 5 is dedicated to experimental results and finally Section 6 draws conclusions.
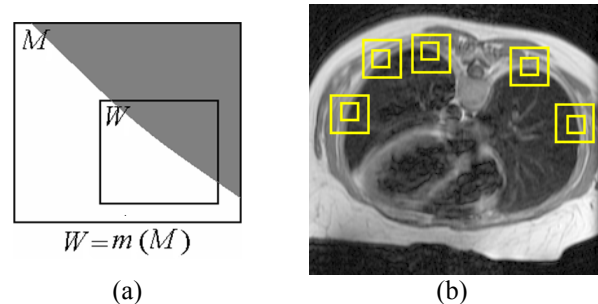
Fig. 1. (a) A contractive self-affine map and (b) a self-affine model with $\zeta=5$ square domains.

2. Self-Affine Mapping System

Consider an image having the support $G \subset R^2$ with the intensity $I(\boldsymbol{x})$ for all $\boldsymbol{x}=(x,y) \in G$. The contractive self-affine map m with the domain $M \subset G$ is defined as follows:

$$\boldsymbol{x}_\omega = m(\boldsymbol{x}) = r(\boldsymbol{x} - \bar{\boldsymbol{x}}_m) + \bar{\boldsymbol{x}}_\omega, \qquad r<1 \qquad (1)$$

where $\bar{\boldsymbol{x}}_m$ and $\bar{\boldsymbol{x}}_\omega$ are the center points of the domains M and W, respectively, and we have:

$$\bar{\boldsymbol{x}}_\omega = \bar{\boldsymbol{x}}_m + \boldsymbol{\tau} \qquad (2)$$

In other word, Equation (1) translates M by the vector $\boldsymbol{\tau}=(s,t)$ and contracts it by the coefficient r to make the domain $W=m(M)$ as illustrated in Fig. 1.a. A contractive self-affine model is defined by $\{M,m,u\}$ where:

$$u(z) = pz+q, \qquad z = I(\boldsymbol{x}_\omega), \qquad 0 \le p \le 1 \qquad (3)$$

In order to maintain the self-similarity conditions, the identity map is usually used for u (*i.e.* $p=1$ and $q=0$). Furthermore, the scaling coefficient r is usually constant to simplify computations.

Similarly, an expanding self-affine map is defined by $\{W,\omega,v\}$ where $\omega=m^{-1}$ and $v=u^{-1}$ with $r>1$. The inverse of each contractive self-affine map is an expanding self-affine map and vice versa which means that:

$$\boldsymbol{x}_m = \omega(\boldsymbol{x}) = \frac{1}{r}(\boldsymbol{x} - \bar{\boldsymbol{x}}_\omega) + \bar{\boldsymbol{x}}_m \qquad (4)$$

The process of extracting self-affine maps includes two steps. First, some domains (M or W) are allocated. The domain allocation method depends on the application of self-affine model. Then, for each self-affine map, the matching algorithm changes the value of one parameter in every step and subsequently, the following matching cost is evaluated [1]:

$$\psi_W(\boldsymbol{\tau}) = \iint\limits_{x\in W}\left(I(\boldsymbol{x})-I(\boldsymbol{x}_m)\right)^\lambda dx\,dy \qquad (5)$$

where λ is an even integer. After checking all possible situations, the optimal parameters with the minimum cost are obtained as follows:

$$\tilde{\boldsymbol{\tau}} = \arg\min_{-k<s,t<k}\left(\psi(\boldsymbol{\tau})\right) \qquad (6)$$

The duplicate of ψ_W can be obtained by replacing $\boldsymbol{x}$ with $m(\boldsymbol{x})$ as follows:

$$\psi_M(\boldsymbol{\tau}) = \iint\limits_{x\in M}\left(I(\boldsymbol{x})-I(\boldsymbol{x}_\omega)\right)^\lambda dx\,dy \qquad (7)$$

such that

$$\psi_M(\boldsymbol{\tau}) = \frac{1}{r^2}\psi_W(\boldsymbol{\tau}) \qquad (8)$$

In the above equation, the coefficient $1/r^2$ is constant therefore, both ψ_W and ψ_M have the same optimums.

Fig. 1.b illustrates a self-affine model with square domains of size $K\times K$, $\zeta=5$, and $r=0.5$. According to (6), the possible values of s and t for the matching algorithm were chosen in the range $[-k,k]$ where $k=K/2$. As shown, the texture in each larger block (M) is almost similar to that in the corresponding smaller block W.

3. Analytical Principles

Considering (2) and (4), the first order derivative of ψ_W with respect to $\boldsymbol{\tau}$ is given by:

$$\frac{d\psi_W(\boldsymbol{\tau})}{d\boldsymbol{\tau}} = \frac{\lambda}{r}\int\limits_{x\in W}\int\left(I(\boldsymbol{x})-I(\boldsymbol{x}_m)\right)^{\lambda-1}\left(\frac{dI(\boldsymbol{x}_m)}{d\boldsymbol{x}_m}\right)dx\,dy \qquad (9)$$

Obviously, the solutions of (6) are the roots of the following equation:

$$\frac{d\psi_W(\boldsymbol{\tau})}{d\boldsymbol{\tau}} = 0 \qquad (10)$$

As maintained by triangular inequality [8], we have

$$0\le\left\|\frac{d\psi_W(\boldsymbol{\tau})}{d\boldsymbol{\tau}}\right\|\le\frac{\lambda}{r}\int\limits_{x\in W}\int\left|I(\boldsymbol{x})-I(\boldsymbol{x}_m)\right|^{(\lambda-1)}\left\|\frac{dI(\boldsymbol{x}_m)}{d\boldsymbol{x}_m}\right\|dx\,dy \qquad (11)$$

where $\|.\|$ is Minkowski's distance of the second rank [9]. According to the sandwich theorem [8], in the above expression, the roots of the right term are also the roots of the central one. Therefore, we can compute some solutions of (11) by solving the following equation:

$$\int\limits_{x\in W}\int\left|I(\boldsymbol{x})-I(\boldsymbol{x}_m)\right|^{(\lambda-1)}\left\|\frac{dI(\boldsymbol{x}_m)}{d\boldsymbol{x}_m}\right\|dx\,dy = 0 \qquad (12)$$

Considering this fact that both terms of the above integral are not negative, the answers ($\tilde{\boldsymbol{\tau}}$) of (12) should satisfy one of the following conditions for each $\boldsymbol{x}$:

$$\forall \boldsymbol{x}\in W, \tilde{\boldsymbol{\tau}}: \quad \begin{aligned}(a) &\left.\left\|\frac{dI(\boldsymbol{x}_m)}{d\boldsymbol{x}_m}\right\|=0\right| \\ (b) &\left.I(\boldsymbol{x}_m)=I(\boldsymbol{x})\right|_{\boldsymbol{x}_m\in M}\end{aligned} \qquad (13)$$

The first condition usually remains satisfied in smoothed regions. Therefore, only the edges of M (with significant gradient amplitude) take part in computing the optimal

parameters. In this case, for any edge point of M, we have:

$$\exists \boldsymbol{x}\in W, \left\|\frac{dI(\boldsymbol{x}_m)}{d\boldsymbol{x}_m}\right\|\ne 0: \quad I(\boldsymbol{x}_m)=I(\boldsymbol{x}) \qquad (14)$$

Generally, the above equation will remain valid for a number of edge points if, and only if:

$$\boldsymbol{x}=\boldsymbol{x}_m \Rightarrow \boldsymbol{x}=\frac{1}{r}(\boldsymbol{x}-\bar{\boldsymbol{x}}_\omega)+\bar{\boldsymbol{x}}_\omega-\tilde{\boldsymbol{\tau}} \Rightarrow \tilde{\boldsymbol{\tau}}=\frac{1-r}{r}(\boldsymbol{x}-\bar{\boldsymbol{x}}_\omega) \qquad (15)$$

Considering this fact that $\tilde{\boldsymbol{\tau}}$ is independent of $\boldsymbol{x}$, the following consequence can be straightforwardly drawn:

$$r=1 \Rightarrow \tilde{\boldsymbol{\tau}}=\boldsymbol{0} \qquad (16)$$

However, this obvious solution is disadvantageous, because it reduces the self-affine map to an identical map. In the following subsections, first, we solve (6) for one edge-line-segment (ELS) and multiple convergent ELSs. Then, the results are extended to the general case.
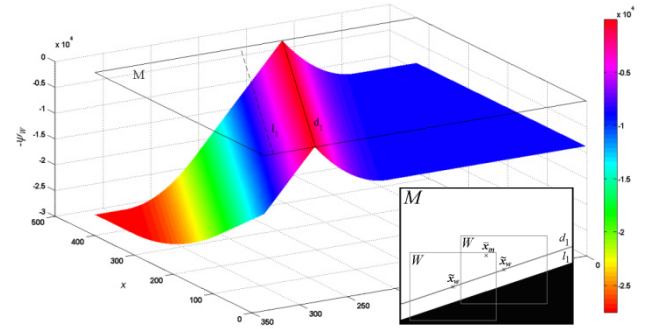
Fig. 2. Variations of $-\psi_W$ versus different W-centers inside M. The domain M includes one ELS (l_1) while the corresponding locus of OCW (with $r=0.5$) is indicated by the LLS d_1 which is parallel to l_1. (b)

3.1 One Edge-Line-Segment

Suppose that the domain M includes only one ELS as follows:

$$l_i: \quad y = a_i x + b_i \qquad i=1,2,\ldots,n \qquad (17)$$

where n is the total number of ELSs, here $n=1$. As illustrated in Fig. 2, for all points of M except those on l_i, we have:

$$\forall \boldsymbol{x}_m\notin l_i: \quad \frac{dI(\boldsymbol{x}_m)}{d\boldsymbol{x}_m}=0 \qquad (18)$$

In this case, Eq. (14) will be valid if, and only if:

$$\forall \boldsymbol{x}_m\in l_i: \quad \boldsymbol{x}=m(\boldsymbol{x}_m)\in l_i \qquad (19)$$

Hence,

$$\boldsymbol{x}\in l_i \Rightarrow y = a_i x + b_i \Rightarrow$$
$$r(y_m-\bar{y}_m)+\bar{y}_m+\tilde{t}=a_i[r(x_m-\bar{x}_m)+\bar{x}_m+\tilde{s}]+b_i \Rightarrow$$
$$y_m = \frac{1}{r}[a_i r(x_m-\bar{x}_m)+a_i\bar{x}_m-\bar{y}_m+a_i\tilde{s}-\tilde{t}+b_i]+\bar{y}_m \Rightarrow$$
$$y_m = a_i x_m + \frac{1}{r}[a_i(1-r)\bar{x}_m-(1-r)\bar{y}_m+(a_i\tilde{s}-\tilde{t})+b_i] \qquad (20)$$

Eq. (21) is easily concluded from (17), (19), and (20) as follows:

$$b_i = \frac{1}{r}[a_i(1-r)\bar{x}_m-(1-r)\bar{y}_m+(a_i\tilde{s}-\tilde{t})+b_i] \Rightarrow$$
$$D_i: \quad \tilde{t}=a_i\tilde{s}-(1-r)(\bar{y}_m-a_i\bar{x}_m-b_i) \qquad (21)$$

where the line D_i is the locus of optimal translation vectors corresponding to d_i and obviously, we have:

$$\tilde{\boldsymbol{\tau}}\in D_i: \quad \left.\frac{d\psi_W(\boldsymbol{\tau})}{d\boldsymbol{\tau}}\right|_{\tau=\tilde{\tau}}=0 \qquad (22)$$

Furthermore, according to (2) and (21), the locus of optimal centers of the domain W (OCW) is given by:

$$d_i: \quad \tilde{y}_\omega = a_i \tilde{x}_\omega + \hat{b}_i \tag{23}$$

where $\tilde{x}_\omega = (\tilde{y}_\omega, \tilde{x}_\omega)$ indicates the optimum center of W (i.e. $\tilde{x}_\omega = \bar{x}_m + \tilde{\tau}$) and $\hat{b}_i$ is given by:

$$\hat{b}_i = b_i + r(\bar{y}_m - a_i \bar{x}_m - b_i) \tag{24}$$

In the above equation, if the ELS l_i passes through the center point of M, .i.e. $\bar{x}_m = (\bar{y}_m, \bar{x}_m)$, the second term will be zero and hence, d_i will be fitted to l_i. Obviously, both of the locus-line-segments (LLSs) D_i and d_i are parallel to the ELS l_i, all with the same slope of a_i.

The function $\phi_i(x)$ computes the algebraic non-normalized distance of x from the line l_i as follows:

$$\phi_i(x) = y - a_i x - b_i \tag{25}$$

The corresponding Euclidian distance is given by:

$$\Phi_i(x) = \frac{|\phi_i(x)|}{\sqrt{1 + a_i^2}} \tag{26}$$

By using (1), (4), and (25), the following equations can simply be drawn:

$$\forall x \in M: \quad \phi_i(x_\omega) = r\phi_i(x) + \left(\phi_i(\bar{x}_\omega) - r\phi_i(\bar{x}_m)\right) \tag{27}$$

$$\forall x \in W: \quad \phi_i(x) = r\phi_i(x_m) + \left(\phi_i(\bar{x}_\omega) - r\phi_i(\bar{x}_m)\right) \tag{28}$$

Furthermore, for the optimal center of W given by (23) and (24), we have:

$$\phi_i(\tilde{x}_\omega) = \tilde{y}_\omega - a_i \tilde{x}_\omega - b_i = \hat{b}_i - b_i = r(\bar{y}_m - a_i \bar{x}_m - b_i) = r\phi_i(\bar{x}_m) \tag{29}$$

It means that by using the optimal center $\tilde{x}_\omega$, the second term of (27) and (28) vanishes and we have:

$$\forall x \in M: \quad \phi_i(x_\omega) = r\phi_i(x) \tag{30}$$

$$\forall x \in W: \quad \phi_i(x) = r\phi_i(x_m) \tag{31}$$

Consequently, once each point of M ($x \in M$) is mapped through an optimal contractive (expanding) self-affine map, its distance to l_i is decreased (increased) by the coefficient r. Besides, as shown in the last two equations, the signs of $\phi_i(x)$, $\phi_i(x_\omega)$, and $\phi_i(x_m)$ are the same which means that all of x, x_ω, and x_m are located at the same side of l_i. Therefore, the following consequence can be easily drawn:

$$\tilde{\tau} = \tilde{x}_\omega - \bar{x}_m \Rightarrow \psi_W(\tilde{\tau}) = \psi_M(\tilde{\tau}) = 0 \tag{32}$$

It means that every optimal center of W which is located on d_i determines a zero-minimum of ψ. Therefore, the following lemma can be straightforwardly drawn from the above analytical justifications.

Lemma I. *In a self-affine map, if the domain M includes only one edge-line-segment (ELS) as given by (17) with n=1, we will have:*

- *The locus of optimal centers of W consists of a line-segment parallel to ELS as indicated by (23).*
- *Attraction and repellence behaviors: Once each point of M is mapped through an optimal contractive (expanding) self-affine map, its distance to ELS is decreased (increased) by the coefficient r according to (30) and (31).*
- *As shown in (32), each optimal center of W determines a zero-minimum of the cost function ψ_W.*

The above lemma is further illustrated in Fig. 2. In this figure, the values of -ψ_W for different W-centers inside M

are shown. The margins of the domain M, ELS l_1 (indicated by dashed lines), and LLS d_1 are also indicated. As shown, the optimal centers of W are located on d_1 which is parallel to l_1 with ψ_W=0.
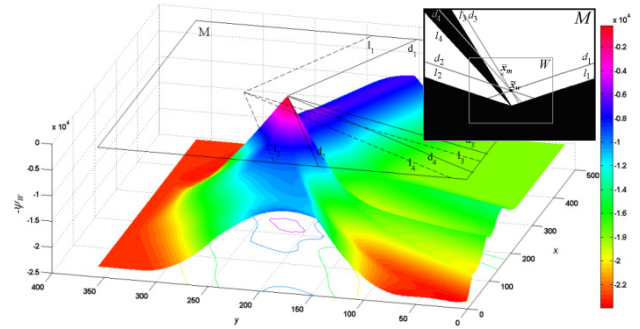
Fig. 3. Variations of -ψ_W versus different W-centers inside M. The domain M includes four convergent ELSs (i.e. l_1 to l_4). Corresponding to each ELS (l_i), there is a parallel LLS (d_i) with r=0.5. LLSs are convergent to the optimal center $\tilde{x}_\omega$ of W because of convergent ELSs.
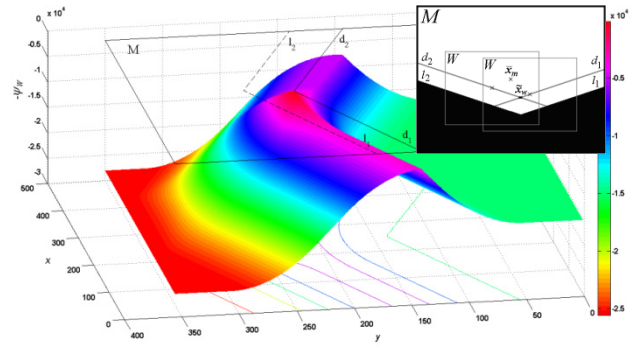
Fig. 4. Variations of -ψ_W versus different W-centers inside M. The domain M includes two intersecting ELSs (i.e. l_1 and l_2). Corresponding to each ELS (l_i), there is a parallel LLS (d_i) with r=0.5.

3.2 *Multiple Convergent Edge-Line-Segments*

Consider that M includes n ELSs according to (17) therefore; corresponding to each l_i, the locus of OCW (d_i) is given by (23).

Obviously, ψ_W will include a zero-minimum if, and only if, the following equations set are consistent:

$$\begin{cases} d_1: & \tilde{y}_\omega = a_1 \tilde{x}_\omega + \hat{b}_1 \\ d_2: & \tilde{y}_\omega = a_2 \tilde{x}_\omega + \hat{b}_2 \\ \vdots \\ d_n: & \tilde{y}_\omega = a_n \tilde{x}_\omega + \hat{b}_n \end{cases} \tag{33}$$

It means that there is an optimal center for W which observes all the above equations only when the whole of ELSs are convergent to one point as illustrated in Fig. 3. In more details, if all ELSs pass through the point $\tilde{x}_m$, we will have:

$$\forall i = 1, 2, ..., n: \quad \phi_i(\tilde{x}_m) = 0 \tag{34}$$

Besides, according to (23), (24), and (29), the optimal center of W which is also a solution of (33) observes the following equation for each ELS:

$$\forall i = 1, 2, ..., n: \quad \phi_i(\frac{\tilde{x}_\omega - r\bar{x}_m}{1 - r}) = 0 \tag{35}$$

Hence, $\tilde{x}_\omega$ can be given by:

$$\tilde{x}_m = \frac{\tilde{x}_\omega - r\bar{x}_m}{1 - r} \Rightarrow \tilde{x}_\omega = r\bar{x}_m + (1 - r)\tilde{x}_m \tag{36}$$

According to the above equation, the optimal W-center is obtained as the weighted average of the cross-point ($\tilde{x}_m$) and the center of M ($\bar{x}_m$).

For example, when M includes two intersecting ELSs (i.e. $a_1 \neq a_2$) as illustrated in Fig. 4, the unique optimal center of W (with $\psi_W = 0$) is given by:

$$\tilde{s} = -(1-r)\left(\frac{b_1 - b_2}{a_1 - a_2} + \bar{x}_m\right), \tilde{t} = -(1-r)\left(\frac{a_2 b_1 - a_1 b_2}{a_1 - a_2} + \bar{y}_m\right) \quad (37)$$

The center of W should be located inside M as follows:

$$k < \tilde{s}, \tilde{t} < k \quad (38)$$

The center of M can be determined as $\bar{x} = \bar{y} = k$ therefore, using (37) and (38), we have:

$$-k < (1-r)(\gamma_j - k) < k, \qquad j = 1,2 \quad (39)$$

where γ_j is defined as follows:

$$\gamma_1 = \frac{b_1 - b_2}{a_2 - a_1}, \gamma_2 = \frac{b_1 a_2 - a_1 b_2}{a_2 - a_1} \quad (40)$$

The following conditions can easily be drawn from (39) for contractive and expanding self-affine maps, respectively:

Contractive: $r_{\min} = \max\left(\max_{j=1,2}\left(\frac{\max(\gamma_j - K, -\gamma_j)}{|\gamma_j - k|}\right), 0\right) < r < 1 \quad (41)$

Expanding: $1 < r < r_{\max} = \max\left(\min_{j=1,2}\left(\frac{\max(\gamma_j, -(\gamma_j - K))}{|\gamma_j - k|}\right), 1\right) \quad (42)$

Fig. 5 illustrates the range of acceptable values of r versus different values of γ_j according to the above equations. As shown, the cost function ψ_W more probably includes a zero-minimum when the value of r is closer to one. This consequence is intuitively obvious. Because, according to (23), (24), and (29), by approaching r to one, all LLSs (and their cross-point) moves toward the center of M. Therefore, if even the cross-point of ELSs is outside M, by using a sufficiently large r, the cross-point of the corresponding LLSs will be within M.

The variations of $-\psi_W$ versus different W-centers inside M are illustrated in Fig. 4. The optimal W-center is located on the cross-point of d_1 and d_2 with $\psi_W = 0$.

We can extent the conditions of (41) and (42) for the more general case of n ELSs. In more details, $\tilde{x}_\omega$ will be located inside M if, and only if, the conditions of (43) and (44) remain satisfied for contractive and expanding self-affine maps, respectively:

$$r_{\min} = \max\left(\max_{p,q,j}\left(\frac{\max(\gamma_{pqj} - K, -\gamma_{pqj})}{|\gamma_{pqj} - k|}\right), 0\right) < r < 1 \quad (43)$$

$$1 < r < r_{\max} = \max\left(\min_{p,q,j}\left(\frac{\max(\gamma_{pqj}, -(\gamma_{pqj} - K))}{|\gamma_{pqj} - k|}\right), 1\right) \quad (44)$$

where the coefficients γ_{pq1} and γ_{pq2} are defined for each pair of ELSs (e.g. l_p and l_q) as follows:

$$\gamma_{pq1} = \frac{b_p - d_q}{a_q - a_p}, \gamma_{pq2} = \frac{b_p a_q - a_p d_q}{a_q - a_p} \quad (45)$$

According to the above discussion, the following lemma can be straightforwardly drawn.

Lemma II. *If the domain M of a self-affine map includes multiple convergent ELSs as given by (17), we will have:*
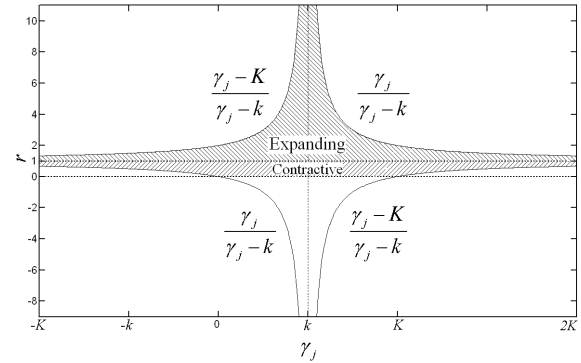
Fig. 5. The range of acceptable values of r versus different values of γ_j for contractive and expanding self-affine maps when M includes two ELSs.

- *The convergent point obtained by solving the equations set of (33) will be the optimal center of W, if the conditions of (44) and (45) remain satisfied.*
- *The above optimal center determines a zero-minimum of the cost function ψ_W.*
- *Attraction and repellence behaviors: Once each point of M is mapped through the contractive (expanding) self-affine map given by using the above optimal center, its distance to the nearest ELS is decreased (increased) by the coefficient r according to (30) and (31).*

Particularly, the last two consequences of the above lemma are straightforwardly inherited from Lemma I, because in this case, the convergent point satisfies all conditions of Lemma I for each ELS, separately. In Fig. 3, the variations of $-\psi_W$ versus different W-centers inside M are illustrated when M includes four ELSs (i.e. d_1 to d_2). As shown, the optimum W-center is located on the convergent point of four LLSs (i.e. l_1 to l_2) with $\psi_W = 0$.

3.3 General Case

Both of the previous lemmas determine the optimal translation vector for the self-affine map when M includes only one ELS or multiple convergent ELSs. These consequences can be further extended as follows.

In the same manner of (9), the following equation can be obtained from (7):

$$\frac{d\psi_M(\boldsymbol{\tau})}{d\boldsymbol{\tau}} = -\lambda \int_{x \in M} \int (I(\boldsymbol{x}) - I(\boldsymbol{x}_\omega))^{\lambda-1}\left(\frac{dI(\boldsymbol{x}_\omega)}{d\boldsymbol{x}_\omega}\right) dxdy \quad (46)$$

By replacing $\boldsymbol{x}_\omega$ by, we have:

$$\frac{d\psi_M(\boldsymbol{\tau})}{d\boldsymbol{\tau}} = \frac{\lambda}{r^2} \int_{x \in W} \int (I(\boldsymbol{x}) - I(\boldsymbol{x}_m))^{\lambda-1}\left(\frac{dI(\boldsymbol{x})}{d\boldsymbol{x}}\right) dxdy \quad (47)$$

Therefore, through (8), (46), and (47), we obtain:

$$\frac{d\psi_W(\boldsymbol{\tau})}{d\boldsymbol{\tau}} = \lambda \int_{x \in W} \int (I(\boldsymbol{x}) - I(\boldsymbol{x}_m))^{\lambda-1}\left(\frac{dI(\boldsymbol{x})}{d\boldsymbol{x}}\right) dxdy \quad (48)$$

Finally, similar to (13), the following equation can be correspondingly drawn:

$$\forall \boldsymbol{x} \in W, \tilde{\boldsymbol{\tau}}: \begin{array}{l} (a) \quad \left\|\frac{dI(\boldsymbol{x})}{d\boldsymbol{x}}\right\| = 0 \\ (b) \quad I(\boldsymbol{x}) = I(\boldsymbol{x}_m) \end{array} \quad (49)$$

Therefore, in the same manner, all previous discussions about ELSs of M can be extended for the ELSs inside W. Consequently, Lemmas I and II can be extended as follows:
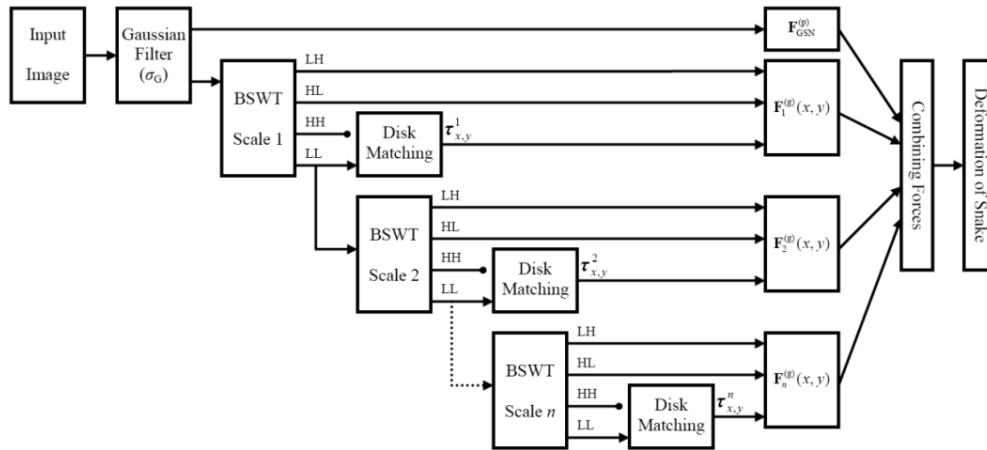
Fig. 6. Block diagram of self-affine snake.

Lemma III. *Consider that in a self-affine map, the domain M includes n ELSs according to* (17). *The optimal center $\tilde{x}_\omega$ of W will be a local minimum of ψ_W, if:*

- *The domain W includes only one ELS and $\tilde{x}_\omega$ is located on the corresponding LLS.*
- *The domain W includes only multiple convergent ELSs and $\tilde{x}_\omega$ is located on the cross-point of the corresponding LLSs.*
- *Attraction and repellence behaviors: Once each point of M is mapped through the above optimal contractive (expanding) self-affine map, its distance to the nearest ELS is decreased (increased) by the coefficient r according to* (30) *and* (31).

3.4 Consequences

Now, we can draw the following consequences through the above analytical justifications:

- As shown in Fig. 2, the cost function ψ_W, sometimes, may have a number of equivalent local minima which should be handled in some applications.
- Optimal contractive and expanding self-affine maps (as described in Lemma III) provide the attraction and repellence behaviours, respectively.
- By decreasing the size of *W*, the probability of including non-convergent ELSs is decreased. Therefore, the conditions of Lemma III may be better satisfied through a smaller *r*, especially, for contractive self-affine maps.

4. Self-Affine Snake

Self-affine snake (SAS) is a remarkable parametric active contour which recently proposed by the authors [6]. In this approach, the wavelet transform and self-affine mapping system were combined to compute a global force field for parametric active contours.

As shown in Fig. 6, SAS includes six steps as follows: *i)* Gaussian filtering, *ii)* computing wavelet coefficients by using biorthogonal spline wavelets [10], *iii)* extracting optimal self-affine maps in each wavelet scale, *iv)* computing self-affine sub-forces in each scale, *v)* combining sub-forces to obtain self-affine force field, and *vi)* snake deformation using dynamic force formulation [11]. For more details, see also [12-13].

4.1 Improving the Cost Function

In SAS, the disk matching algorithm was used for extracting optimal self-affine maps [6]. This method finds the optimal translation vector which minimizes the cost function ψ_W of (5). However, as aforementioned in Subsection 3.3, ψ_W sometimes has multiple equivalent local minima which may produce ambiguity.

In order to tackle the above shortcoming, we suggest the following cost function instead of (5):

$$\psi(\boldsymbol{\tau}_{x,y}) = \exp\left(\frac{\|\boldsymbol{\tau}_{x,y}\|}{2k_d^2}\right)\left(1 + \iint_{x \in M_{x,y}} \|I(\boldsymbol{x}) - I(\boldsymbol{x}_m)\|_\lambda \, dx \, dy\right) \quad (50)$$

where $k_d > 0$ is the distance penalty coefficient and $\boldsymbol{\tau}_{x,y} = (s_{x,y}, t_{x,y})$ indicates the translation vector of the pixel (x,y). Therefore, we have:

$$\begin{cases} \tilde{\psi}_{x,y} = \min_{\boldsymbol{\tau}_{x,y}}\left(\psi(\boldsymbol{\tau}_{x,y})\right) \\ \tilde{\boldsymbol{\tau}}_{x,y} = \arg\min_{\boldsymbol{\tau}_{x,y}}\left(\psi(\boldsymbol{\tau}_{x,y})\right) \end{cases} \quad (51)$$

In Eqn. (50), the second term which computes a positive similarity cost is penalized by the first term that is exponentially related to the length of $\boldsymbol{\tau}_{x,y}$. Therefore, when there are two or more translation vectors with the same similarity cost (Eqn. 5), the shortest one will be intuitively chosen as the optimum vector. In this manner, the enhanced disk matching algorithm can usually make unique answers by using (50) instead of (5).

4.2 Application for Medical Images Segmentation

Self-affine snake is an appropriate candidate for medical images segmentation because of outstanding properties such as:

- Producing promising solutions which are guaranteed by the analytical justifications given in Section 3.
- Wide capture range [6]
- Short CPU time for force field computation and snake deformation [12]
- Remarkable robustness against noise [13]

5. Experimental Results

The results of self-affine snake for 12 medical images are illustrated in Fig.6. These images are indicated as follows:

(a)   A cell image of size 92×104

(b)   A mouth ulcer image of size 78×108
(c)-(g)   Five short-axis magnetic-resonance (MR) images of the left ventricle of the human heart of size 160×160, 128×128, 99×113, 91×91, and 332×332, respectively.
(h)   A MR image of elbow of size 338×338
(i)   Axial T1 weighted MR image of the human shoulder of size 238×243.
(j)   A sagittal oblique angulated T2 weighted MR image of the human shoulder of size 176×206 with fat suppression.
(k)   A MR image of the human chest
(l)   A mamographic image

In each image, compared to deformation curves, the initial and final contours are shown by thicker lines. As shown, SAS could successfully segment the desired boundaries of all medical images.

6. Conclusion

In this paper, the attraction and repellence behaviours of self-affine maps were proved. Besides, we showed that the cost function of a self-affine map, sometimes, may have a number of equivalent optimal minima. Therefore, the cost function of self-affine snake was improved to tackle the above shortcoming as an example. It was shown that SAS is an appropriate active contour for medical image segmentation. Experimental results demonstrated its results for 12 medical images produced by different imaging methods.

References

[1]. M. Barnsley and L. Hurt, *Fractal Image Compression*. Wellesley, MA: Peters, 1993.
[2]. D.M. Monro, F. Dudbridge, and A. Wilson, "Deterministic rendering of self-affine fractals," presented at IEE Colloquium on Application of Fractal Techniques in Image Processing, 1990, pp. 5/1–5/4.
[3]. S. Kumar, K.N. Rao, R.R. Mishra, and R.C. Jain, "An efficient bath fractal transform-based image coding technique," *IEEE Trans. Consumer Electron.*, vol. 44, no. 4, pp. 1298–1308, 1998.
[4]. T. Ida and Y. Sambonsugi, "Image segmentation and contour detection using fractal coding," *IEEE Trans. Circuits Syst. Video Technol.*, vol. 8, no. 8, pp. 968–975, 1998.
[5]. T. Ida and Y. Sambonsugi, "Self-affine mapping system and its application to object contour extraction," *IEEE Trans. Image Processing*, vol. 9, no. 11, pp. 1926–1936, 2000.
[6]. M. Saadatmand-Tarzjan, H. Ghassemian, "Self-affine snake: a new parametric active contour," presented at IEEE Int'l Conf. Signal Processing and Communications, Nov. 2007.
[7]. M. Saadatmand-Tarzjan, H. Abrishami Moghaddam, "A new method for contour extraction based on self-affine mapping system," in *Proc. 2004 Conf. Intelligent Syst*ems. Available: http://saadatmand.synthasite.com/publications.php.
[8]. M.D. Greenbery, *Foundation of Applied Mathematics*. Prentice Hall, 1978.
[9]. S. Theodoridis and K. Koutroumbas, *Pattern Recognition*. San Diego: Academic Press, 2003.
[10]. Daubechies, "Ten lectures on wavelets", *CBMS, SIAM*, vol. 61, pp. 271–280, 1994.
[11]. C. Xu and J.L. Prince, "Snakes, shapes, and gradient vector flow," *IEEE Trans. Image Processing*, vol. 7, no. 3, pp. 359–369, 1998.
[12]. م. سعادتمند طرزجان، ح. قاسمیان،"بهبود مرز فعال خودنسبی برای ناحیه‌بندی تصاویر پزشکی"، ارسال شده برای پذیرش در چهاردهمین کنفرانس انجمن کامپیوتر ایران، ۱۳۸۷.

[۱۳]. م. سعادتمند طرزجان، ح. قاسمیان،"بررسی پایداری مرز فعال خودنسبی در برابر نویز و اهمیت آن در ناحیه‌بندی تصاویر پزشکی"، ارسال شده برای پذیرش در چهاردهمین کنفرانس انجمن کامپیوتر ایران، ۱۳۸۷.

Fig. 7. Results of self-affine snake for 12 medical images.